Turkish Journal of Electrical Engineering & Computer Sciences

http://journals.tubitak.gov.tr/elektrik/

Research Article

Turk J Elec Eng & Comp Sci
(2015) 23: 1834 – 1852
© TÜBİTAK
doi:10.3906/elk-1404-214

Transient stability analysis of VSC HVDC transmission with power injection on the DC-link

Agha Francis NNACHI[1,*], **Josiah MUNDA**[1], **Dan Valentine NICOLAE**[1], **Augustin Mabwe MPANDA**[2]
[1]Department of Electrical Engineering, Tshwane University of Technology, South Africa
[2]Graduate School of Electronics and Electrical Engineers (ESIEE), Amiens, France

Received: 12.04.2014 • **Accepted/Published Online:** 22.06.2015 • **Printed:** 30.11.2015

Abstract: The utilization of a DC-link transmission corridor of embedded VSC HVDC for a DC power injection from renewable energy sources to increase the power flow capability and AC network stability support is a promising technology. However, DC faults on the DC transmission line are likely to threaten the system's operation and stability, especially when the DC power injection exceeds certain limits. A DC single line-to-earth fault is the most likely fault scenario and its effect on the VSC HVDC operation will depend on the earth-loop impedance. Adding an injection point on the DC-link will reduce the earth-loop impedance, hence imposing a danger of increasing the earth fault current. Therefore, in this paper, a VSC HVDC with a DC power injection on the DC-link is studied, the DC-line-to-earth fault is analyzed in the time domain, and its effects on the DC and AC sides of the system are presented. The analysis is based on a developed state-space representation of the system under a single-line-to earth fault. The zero-input zero-state (ZIZS) response is used to find the solution of the state-space representation. In order to correlate the state-space solution with a simulation, the system is modeled in MATLAB/Simulink. Interestingly, it was observed that a quick recharging of the DC-link capacitor due to a power injection created an additional damping of the postfault oscillations of the AC-side power angle and the DC-side voltage and power oscillations, hence enhancing transient stability.

Key words: Transient stability, voltage source converter, DC power injection

1. Introduction

Embedding a voltage source converter high voltage direct current (VSC HVDC) in AC networks opens up new possibilities to enhance the operation of smart transmission grids with improved transient stability, increased power transfer capability, capacity utilization, and delivery efficiency [1]. Moreover, VSC HVDC (HVDC plus or HVDC light) with a long DC transmission link in power systems will facilitate power injections and tap-offs on the DC-link resulting in multiterminal systems for more power transfer capability, support, and supply to disperse rural or electrification loads [2]. The technology of multiterminal HVDC systems has been considered in the literature [3–7] with the view of control coordination among all terminal stations.

However, most of the VSC HVDC systems are two-terminal or point-to-point connection. Here are several examples: 300 MW, 350 kV Caprivi link of Namibia; 400 MW, 200 kV US-East Bay Oakland; 400 MW, 150 kV NordE.ON1 Germany; 350 MW, 150 kV Estlink Estonia Finland-Espoo; 200 MW, 150 kV Murray link Australia; etc. These two-terminal DC-links were generally not designed for the connection of distributed generators [8].

*Correspondence: nnachiaf@tut.ac.za

Connecting a generation scheme to any transmission or distribution system entails taking into consideration certain technical issues such as [9,10]: the thermal rating of the equipment, system fault levels, stability, reverse power flow capability, line-drop compensation, steady-state voltage rises, losses, power quality (such as flicker, harmonics), and protection. The main requirement for a DC power injection on the DC-link transmission corridor of VSC HVDC is injecting a strictly locally controlled power that will not interfere with the main HVDC system control.

In [11], using the principle of uniform loading, a DC power injection limit that could be accepted at any point on the DC-link of a VSC HVDC transmission corridor without affecting the main VSC HVDC control was proposed. However, there is a need to investigate the transient stability of this system during power injection. The degree of transient stability will depend on the location and nature of the disturbance in addition to the initial operating point [12].

Faults may occur at the AC side of the VSC HVDC transmission or on the DC-link transmission corridor, and their stability responses will differ. In [13], it was indicated that if a severe disturbance threatens the system's transient stability on the AC side, the VSC HVDC can help maintain a synchronized power-grid operation by fast power run-up or run-back control functions. On the other hand, VSCs are vulnerable to DC cable short-circuits and ground faults due to a high discharge current from the DC-link capacitance. Therefore, DC faults on the DC transmission line are likely to threaten the system's operation and stability, especially when the DC power injection exceeds a certain limit.

The effect of this DC-line-to-earth fault on the VSC HVDC operation will also depend on the earth-loop impedance. Various works [14–16] have been carried out on power injection or tapping on the DC-link of the VSC HVDC transmission, but the transient stability of the system under DC fault conditions needs to be addressed. Moreover, most researchers [17–19] have based their DC fault analyses on simulations alone.

In this paper, a time-domain transient stability analysis of VSC HVDC during power injection is presented. In the analysis, a state-space representation of a DC-link single-line-to-ground fault during DC power injection is developed. In addition, the zero-input zero-state (ZIZS) response is used to find the solution of the state-space representation. In order to correlate the time-domain solution with a simulation, a two-terminal VSC HVDC with a DC link power injection is developed in the MATLAB/Simulink environment for this study.

2. A VSC HVDC system with DC-power injection

Figure 1 shows a typical embedded VSC HVDC that consists of two main converter stations; one station operates as a rectifier and the other operates as an inverter station. The coordination of active power control between the stations is realized by designing only one converter that controls the DC-side voltage, whereas the other converter regulates the active power. A constant DC voltage control gives a slack bus, which will result in an automatic balance of active power flow between stations [20]. The injection station has its own local control, which should not interfere with the main converter controls. The generator is in stable operation at a phase angle of δ_1 compared with the VSC bus, i.e. the voltage at generator bus E_1 is leading the voltage at converter bus U_1 by an angle of δ.

Introducing DC power on the DC-link and increasing its power injection could reach such an extent that the direction of power flow of the main system could be reversed, causing a net voltage rise at the injection bus and leading to instability.

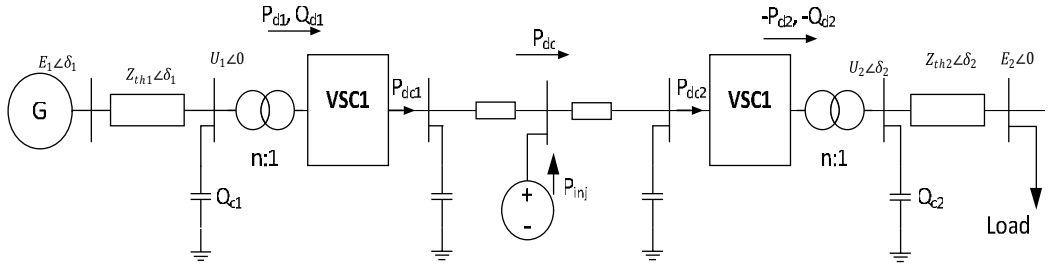

Figure 1. A VSC HVDC with a single machine connected infinite bus having a DC power injection station on the DC-link.

The proposed injection limit is a function of the control parameters of the main converter and the DC-link parameter as shown in Eq. (1).

$$P_{inj\_limit} = \varepsilon P_{ref}, \tag{1}$$

where

$$\varepsilon = -\frac{U_{dcmax}\left(U_{dcmax} - U_{dcref}\right)}{rx} + \left(1 - \frac{x}{2L}\right) U_{dc2} I_{dc2}$$

$$= -\frac{U_{dcmax}\left(U_{dcmax} - U_{dcref}\right)}{rx} + \left(1 - \frac{x}{2L}\right) \frac{U_2 E_2}{X_{th}} sin\delta_2.$$

P_{inj_limit} = the maximum power injection for unity reference power of the main control
U_{dcmax} = the upper voltage regulation limit in p.u. specified in the control
U_{dcref} = the reference voltage in p.u.
r = resistance per kilometer of the line
x = the distance to the injection station from bus 1
L = total length of the DC-link
U_2 = converter AC2 output voltage
E_2 = AC2 bus voltage
X_{th} = the thevenin equivalent reactance of the AC system
U_{dc2} = p.u. upper voltage regulation (limit in p.u specified in the inverter control)
$I_{dc2} = I_{rated}$ = p.u. current reference limit (current set point specified in the inverter control)

3. VSC system DC faults

It is quite true that numerous precautions are taken to ensure the protection of HVDC cables against line faults. Such protections include cable armoring and insulation for submerged cables. However, human and natural factors such as cable deterioration, cable aging, weather, and ocean currents and waves can stress the cable, resulting in insulation breakdowns or potentially broken cables [21]. DC line faults could be line-to-line or line-to-earth faults. However, a single line-to-earth fault is a more likely fault scenario than a line-to-line fault. The occurrence of a DC fault on the DC link of a VSC HVDC will result in fast discharging of the DC-link capacitors and a large AC-side current flowing to the DC link fault point through the antiparalleling (freewheeling) diodes of the converter [22].

4. Transient analysis of a single DC-line-to-earth fault

4.1. State-space representation during a DC power injection

In this section, a transient response from a state-space representation of a single DC-line-to-earth fault during a DC power injection is presented.

The behavior of the system (Figure 2) under earth fault depends on the earth-loop impedance. As a result, the analysis of the single-line earth fault depends on the earthing system of both the main stations and the injection station. The possible earthing points are the neutral of the step-up transformer, the earthing of the DC link midpoint, and the earthing of the injection station. An earth fault will form an earth loop with the earthing of these earthing points [22].

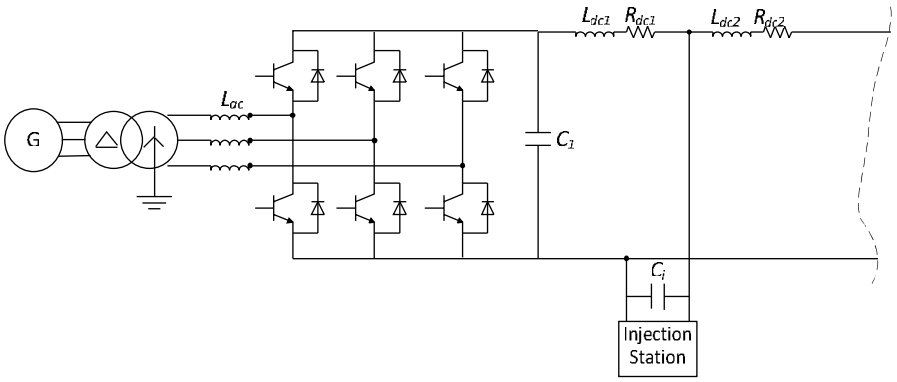

Figure 2. A voltage source converter HVDC with an injection station on the DC-link.

When a line-to-earth fault occurs, the voltage at the point of fault drops significantly, resulting in a high DC fault current. This rise in the DC fault current will result in blocking the IGBTs and hence a rise in the AC fault current. The blocked voltage source will act like an uncontrolled rectifier with the DC-link voltage changing to the rectified voltage, so the current will flow through the diodes as shown in Figure 3. Figure 4 shows the equivalent circuit for the VSC HVDC with a DC power injection under a DC line to earth fault. The earth fault resistance R_f is usually from ohms to hundreds of ohms [23]. The line is modeled by a lumped parameter R-L element.

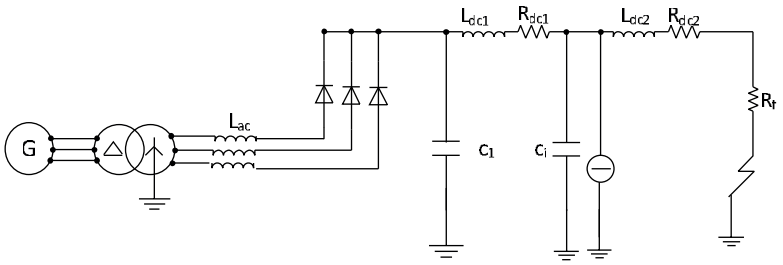

Figure 3. An equivalent circuit of the VSC as a result of blocking the IGBTs.

In order to analyze the response of the system, zero-input and zero-state solutions of the system can be found if the state space representation is known.

Therefore, the state space of the equivalent circuit can be derived in state space as follows:

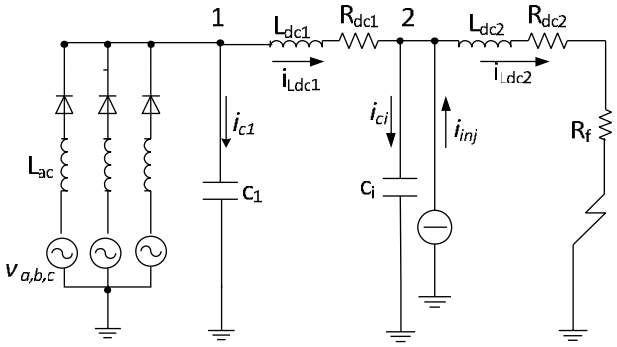

Figure 4. An equivalent circuit of the VSC HVDC with a power injection on DC-link during a DC-line earth fault.

Applying Kirchhoff's laws on each node:

Node 1:

$$i_{c1} = i_{Lac} - i_{Ldc1} \Rightarrow C_1 \frac{dv_{c1}}{dt} = -i_{Ldc1} + i_{Lac} \tag{2}$$

$$v_{Ldc1} = v_{c1} - v_{ci} - v_{Rdc1} \Rightarrow \frac{di_{Ldc1}}{dt} = \frac{1}{L_{dc1}} \left(v_{c1} - v_{ci} - R_{dc1}\, i_{Ldc1} \right); \tag{3}$$

Node 2:

$$i_{c2} = i_{Ldc1} + i_{inj} - i_{Ldc2} \Rightarrow C_2 \frac{dv_{ci}}{dt} = i_{Ldc1} + i_{inj} - i_{Ldc2}$$

$$\Rightarrow \frac{dv_{ci}}{dt} = \frac{i_{Ldc1} + i_{inj} - i_{Ldc2}}{C_2} \tag{4}$$

$$v_{Ldc2} = v_{ci} - v_{Rf} - v_{Rdc2} \Rightarrow L_{dc2} \frac{di_{Ldc2}}{dt} = v_{ci} - i_{Ldc2} \left(R_{dc2} + R_f \right)$$

$$\Rightarrow \frac{di_{Ldc2}}{dt} = \frac{v_{ci}}{L_{dc2}} - i_{Ldc2} \frac{\left(R_{dc2} + R_f \right)}{L_{dc2}} \tag{5}$$

$$v_{Lac} = -v_{c1} + v_{g\,a,b,c} \Rightarrow L_{ac} \frac{di_{Lac}}{dt} = -v_{c1} + v_{g\,a,b,c}. \tag{6}$$

Since the aim here is to monitor the response of the DC-link voltages and currents and the AC current, the state variables v_{c1}, $v_{ci} i_{Ldc1}$, i_{Ldc2}, i_{Lac} can be solved analytically in the time domain or s-domain. Hence, from Eqs. (2)–(6), the state space of the system is defined by the following equation:

$$\left.\begin{array}{l} \dot{x}\,(t) = Ax\,(t) + Bu\,(t) \\ y\,(t) = Cx\,(t) + Du\,(t) \end{array}\right\}, \tag{7}$$

where:

x is the state vector $[v_{c1},\, v_{ci}, i_{Ldc1},\, i_{Ldc2},\, i_{Lac}]^T$,

$\boldsymbol{A}$ is the state matrix $\begin{bmatrix} 0 & 0 & -\frac{1}{C_1} & 0 & \frac{1}{C_1} \\ 0 & 0 & \frac{1}{C_i} & -\frac{1}{C_i} & 0 \\ \frac{1}{L_{dc1}} & -\frac{1}{L_{dc1}} & \frac{R_{dc1}}{L_{dc1}} & 0 & 0 \\ 0 & \frac{1}{L_{dc2}} & 0 & \frac{(R_{dc2}+R_f)}{L_{dc2}} & 0 \\ -\frac{1}{L_{ac}} & 0 & 0 & 0 & 0 \end{bmatrix}$,

$$\boldsymbol{B} \text{ is the input matrix } \begin{bmatrix} 0 & 0 & 0 & 0 & 0 \\ 0 & 1/C_i & 0 & 0 & 0 \\ 0 & 0 & 0 & 0 & 0 \\ 0 & 0 & 0 & 0 & 0 \\ 0 & 0 & 0 & 0 & 1/L_{ac} \end{bmatrix},$$

$$\boldsymbol{u} \text{ is the input } [0,\, i_{inj}, 0,\, 0,\, v_{g\,a,b,c}]^T,$$

$$\boldsymbol{C} \text{ is the output matrix } \begin{bmatrix} 1 & 0 & 0 & 0 & 0 \\ 0 & 1 & 0 & 0 & 0 \\ 0 & 0 & 1 & 0 & 0 \\ 0 & 0 & 0 & 1 & 0 \\ 0 & 0 & 0 & 0 & 1 \end{bmatrix},$$

$\boldsymbol{D}$ is the direct transition (or feed through) matrix $[\mathbf{0}]$, and $\boldsymbol{y}$ is the output.

4.2. Solution of the state space

Having the state matrix, the zero-input (Z_i) and zero-state (Z_s) solution of the system can be found. The zero-input solution is the response of the system to the initial conditions, with the input set to zero. The zero-state solution is the response of the system to the input, with initial conditions set to zero. The complete response is simply the sum of the zero-input and the zero-state responses.

To find the Z_i solution to the system defined in state space, the zero-input problem is given by:

$$\left.\begin{array}{l} \dot{x}_{zi} = Ax \\ y_{zi} = Cx \end{array}\right\}, \tag{8}$$

with a known set of initial conditions, $x\left(0^-\right)$.

The state transition matrix is an important part of both the zero-input and the zero-state solutions of the state space. The state transition matrix in the Laplace domain, ??(s), is defined as:

$$\Phi\left(s\right) = \left(sI - A\right)^{-1}, \tag{9}$$

where I is the identity matrix.

The time-domain state transition matrix, $\varphi\left(t\right)$, is simply the inverse Laplace transform of $\Phi\left(s\right)$.

The first thing is to solve for $x\left(t\right)$ by taking the Laplace transform and solving for $X\left(s\right)$:

$$sX_{zi}\left(s\right) - x\left(0^-\right) = AX_{zi}\left(s\right) \tag{10}$$

$sX_{zi}\left(s\right) - AX_{zi}\left(s\right) = x\left(0^-\right)$ i.e. $sIX_{zi}\left(s\right) - AX_{zi}\left(s\right) = x\left(0^-\right)$

$$\left(sI - A\right)X_{zi}\left(s\right) = x\left(0^-\right)$$

$$X_{zi}\left(s\right) = \left(sI - A\right)^{-1} x\left(0^-\right). \tag{11}$$

Substituting Eq. (9) in Eq. (11),

$$X_{zi}\left(s\right) = \Phi(\mathrm{s})x\left(0^-\right). \tag{12}$$

Since $x\left(0^{-}\right)$ is a constant multiplier, the inverse Laplace Transform is simply

$$x_{zi}\left(t\right)=\varphi\left(t\right)x\left(0^{-}\right). \tag{13}$$

Therefore, the solution for y(t) is found in a straightforward way from the output equation:

$$y_{zi}\left(t\right)=Cx_{zi}\left(t\right)=C\varphi\left(t\right)x\left(0^{-}\right) \tag{14}$$

Next will be to find the zero-state response of the system. In the Laplace domain the response is found by first finding the transfer function of the system:

$$H\left(s\right)=\frac{Y\left(S\right)}{U\left(S\right)}=C\Phi\left(s\right)B+D, \tag{15}$$

$$Y_{zs}\left(S\right)=H\left(s\right)U\left(s\right). \tag{16}$$

In the time domain, Eq. (16) (multiplication in the Laplace domain) yields:

$$y_{zs}\left(t\right)=h\left(t\right)*U\left(t\right)=\left(C\varphi\left(t\right)B+D\right)*u\left(t\right). \tag{17}$$

The asterisk denotes convolution.

Then the complete response is simply the sum of Eqs. (14) and (17):

$$y_{c}\left(t\right)=y_{zi}\left(t\right)+y_{_{zs}}\left(t\right). \tag{18}$$

Table 1 shows the parameters used for plotting the solutions (Eqs. (14), (17), and (18)).

Table 1. Parameters used for plotting the solution in the MATLAB environment.

Elements	Value
Length of DC-link	950 km
Distance from VSC1 bus to injection station bus	475 km
DC-bus capacitor C_1	24 μF
Injection DC-bus capacitor C_i	12 μF
DC-line inductance L_{dc1}	0.00159 $\times$ 475 H
DC-line inductance L_{dc2}	0.00159 $\times$ 125 H
DC-line resistance R_{dc1}	0.00139 $\times$ 475 ohm
DC-line resistance R_{dc2}	0.00139 $\times$ 125 ohm
Earth-fault resistance R_f	0.05 ohm
AC line inductance L_{ac}	0.0487
AC phase voltage V_{ga}	$400/\sqrt{3}$ kV
Initial conditions	$\mathrm{x}\left(0^{-}\right)$ = [6500;1200; 0; 0;0]

Figures 5–8 show the zero-input, zero-state, and combined state solutions or responses of the state variables v_{c1}, $v_{ci}i_{Ldc1}$, i_{Ldc2}, i_{Lac} obtained from Eqs. (14), (17), and (18), respectively.

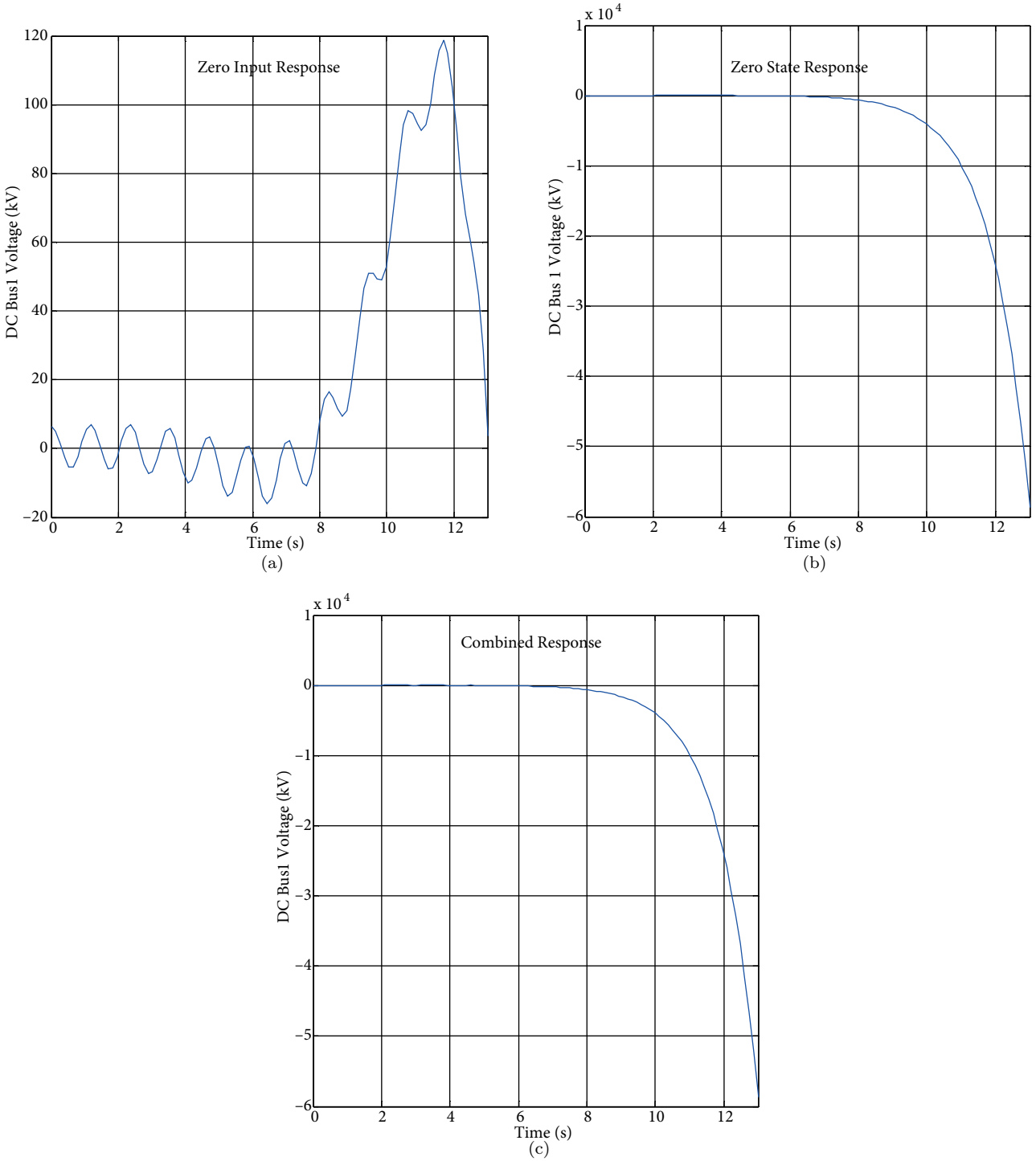

Figure 5. Response of DC bus 1 voltage: a) zero-input response, b) zero-state response, c) combined response.

Figure 5a shows the zero-input response of DC-bus 1 voltage and it can be seen that the capacitor is first charged up to 120 kV due to the initial condition and completely discharged. Figures 5b and 5c show the complete draining of DC bus 1 voltage. Figure 6, which shows the response of the injection station bus voltage, depicts a fast charging up to 800 kV due to the power injection and later discharging completely due to the

line-to-earth fault. Figure 7 shows a fast rise in the DC inductor current, which is a result of the reduced fault loop impedance.

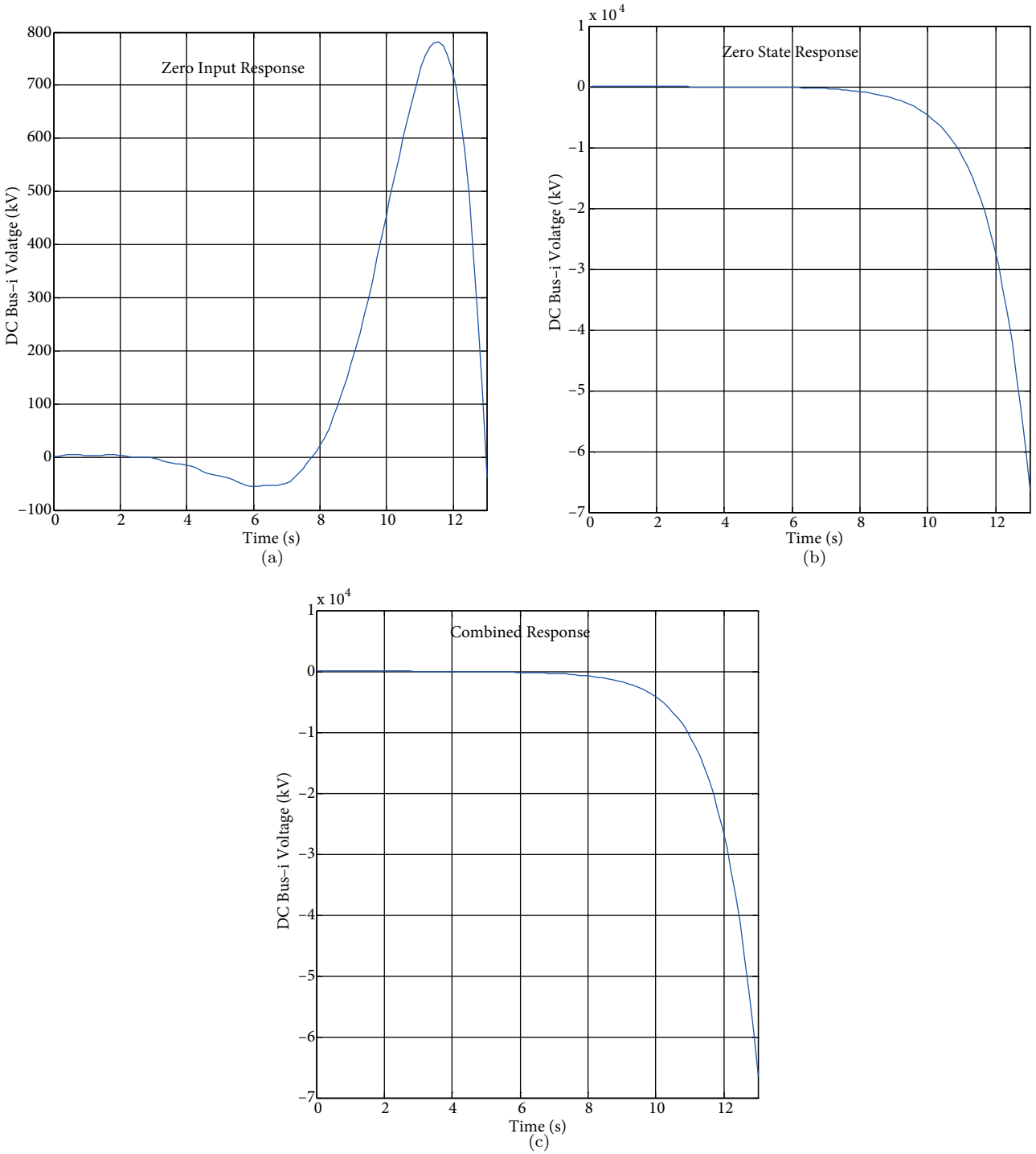

Figure 6. Response of the injection bus voltage: a) zero-input response, b) zero-state response, c) combined response.

More interestingly, Figures 8a–8c show a fast rise in the AC current, which is a result of severe overcurrents due to the discharge of the DC-link capacitances as shown in Figure 8c. Therefore, the converter is defenseless

against DC faults and it is imperative that the protection system, both on the DC and the AC side of the HVDC, should be very fast, reliable, and sensitive during DC system faults.

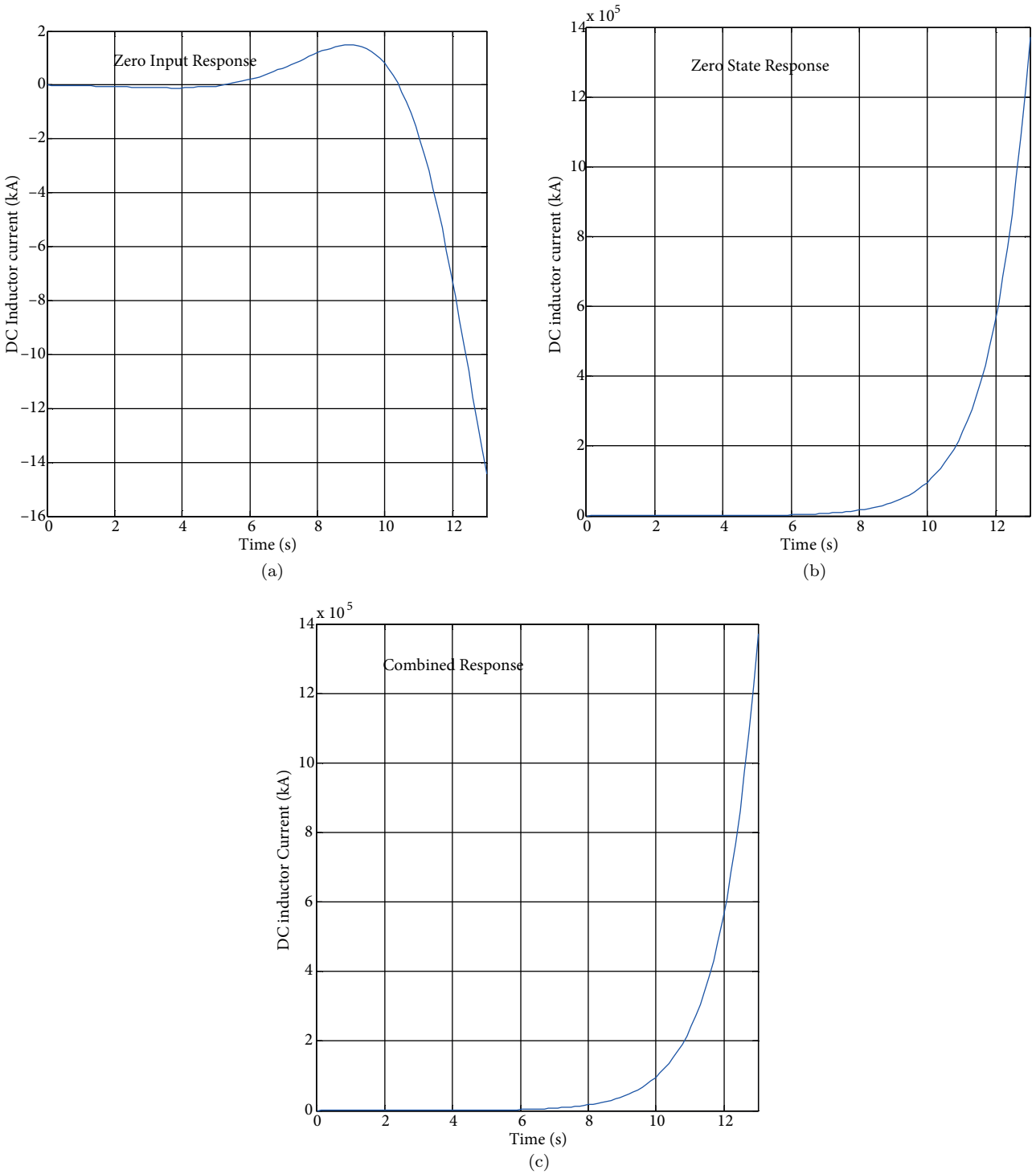

Figure 7. Response of the DC inductor current: a) zero-input response, b) zero-state response, c) combined response.

4.3. State-space representation when there is no DC power injection station

When there is no power injection station, the earth-loop form shared between the injection station, the DC cable, and the AC source is eliminated. This will lead to an increased impedance of the earth-loop, thereby reducing the earth fault current. In this case, the state space reduces to 3 $\times$ 3 with a state vector $x = [v_{c1},\ i_{Ldc},\ i_{Lac}]^T$,

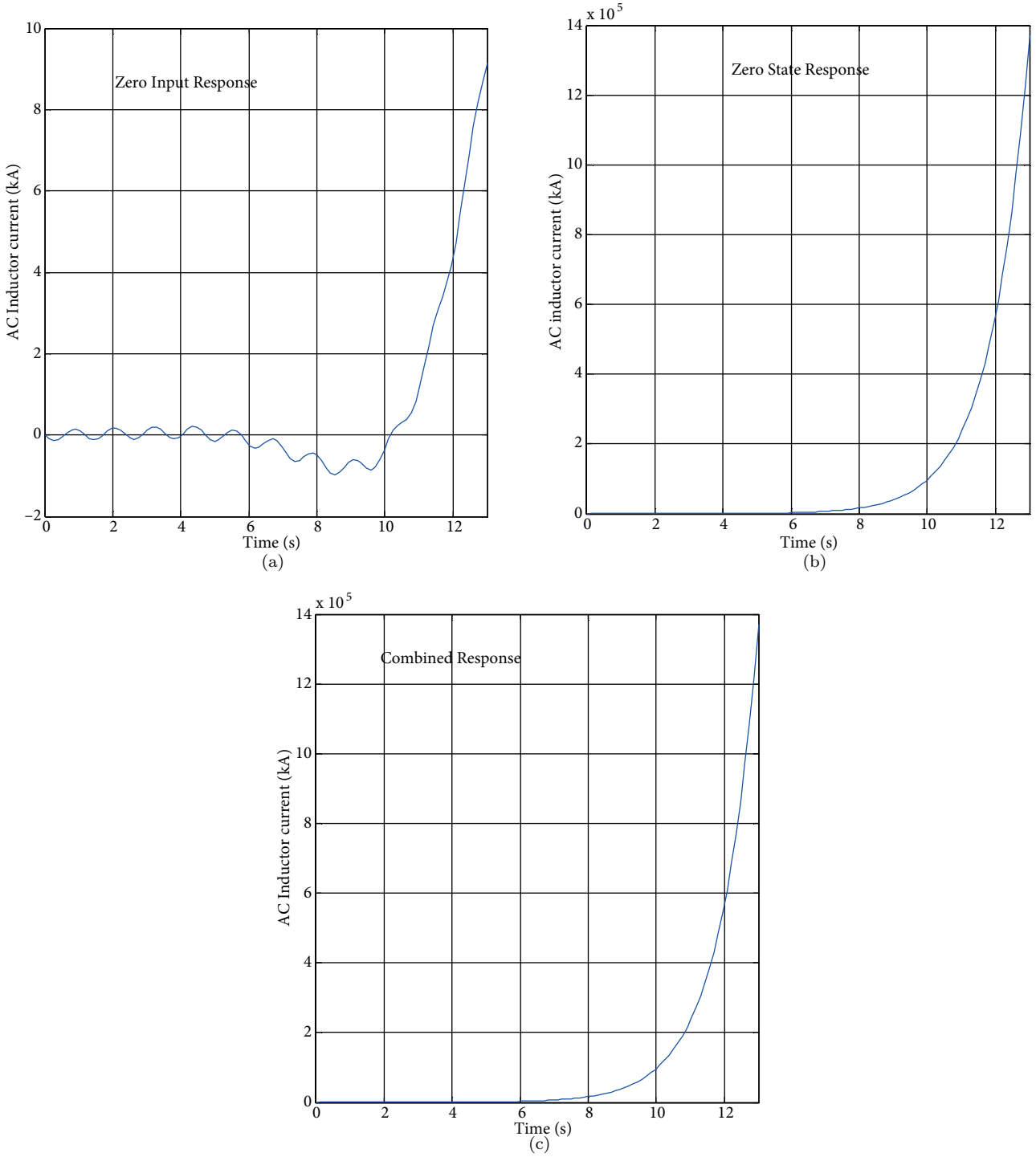

Figure 8. Response of the AC inductor current: a) zero-input response, b) zero-state response, c) combined response.

$$\boldsymbol{A} = \begin{bmatrix} 0 & -\frac{1}{C_1} & \frac{1}{C_1} \\ \frac{1}{L_{dc}} & \frac{-(R_{dc2}+R_f)}{L_{dc2}} & 0 \\ -\frac{1}{L_{ac}} & 0 & 0 \end{bmatrix}, \boldsymbol{B} = \begin{bmatrix} 0 & 0 & 0 \\ 0 & 0 & 0 \\ 0 & 0 & 1/L_{ac} \end{bmatrix}, \boldsymbol{u} = [0,\ 0,\ v_{g\,a,b,c}]^T, \boldsymbol{C} = \begin{bmatrix} 1 & 0 & 0 \\ 0 & 1 & 0 \\ 0 & 0 & 1 \end{bmatrix},$$

$\boldsymbol{D}$ is the direct transition (or feed through) matrix $[\mathbf{0}]$, and $\boldsymbol{y}$ is the output.

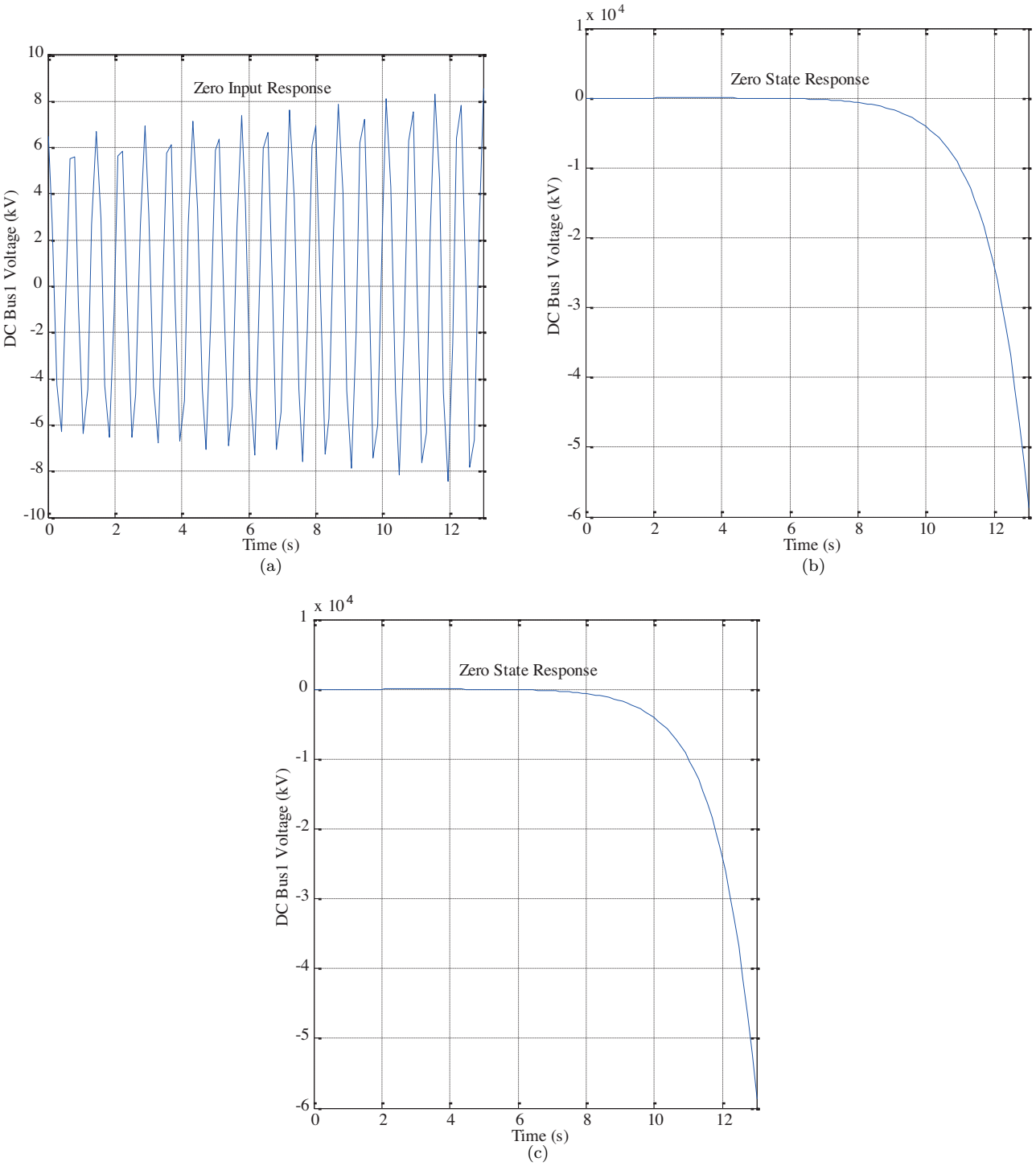

Figure 9. Response of DC bus-1 voltage: a) zero-input response, b) zero-state response, c) combined response.

Figures 9 and 10 show the ZIZS solution of the system. Figure 9a shows an oscillation of the DC bus voltage at a reduced magnitude when compared with Figure 6a. From Figures 9b and 9c, it can be observed that there is a fast and complete drainage of DC bus-1 voltage. Figure 10 shows a fast rise in the AC current with a lesser magnitude of the zero-input response when compared with Figure 8, and this is due to the fact that the earth-loop impedance has increased.

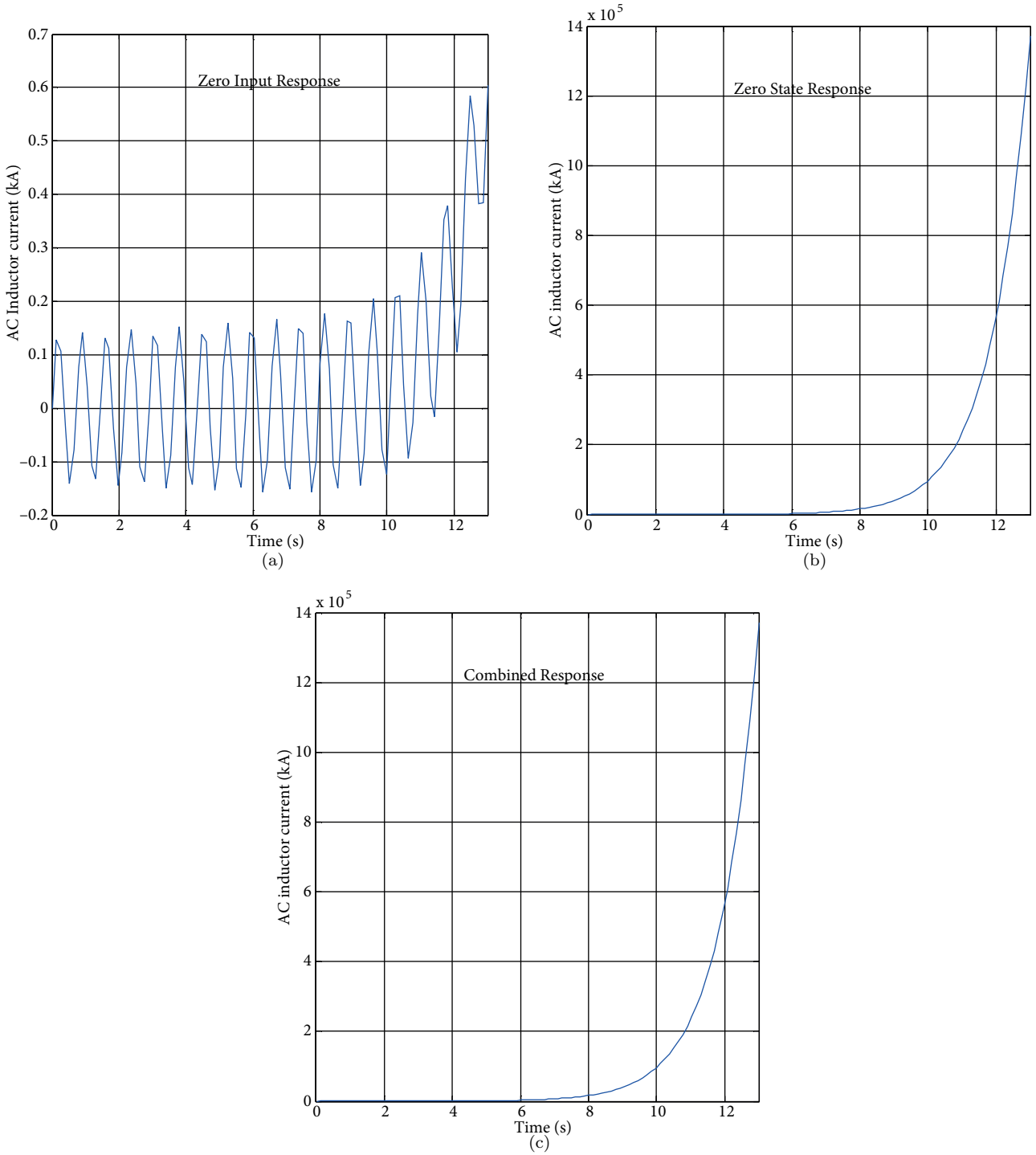

Figure 10. Response of the AC inductor current: a) zero-input response, b) zero-state response, c) combined response.

5. Simulation

To demonstrate the operation of a VSC HVDC with DC power injection under a DC single-line-to-earth fault, a model was developed in the MATLAB/Simulink environment.

Table 2 shows the simulation parameters of a typical 300 MW, 350 kV Caprivi VSC HVDC transmission system used for the modeling in Simulink.

Table 2. Simulation parameters.

Data	Parameters
Power rating	300 MW
Overload rating in monopolar mode	350 MW
No. of poles	1
AC voltage	Gerus: 400 kV; Zambezi: 330 kV
DC voltage	350 kV
Coupling transformer on both sides (Gerus and Zambezi)	315 MVA
Length of overhead DC line	950 km
Switching frequency of converter valve	1150 kHz

The essence of the simulation is to show the effect of DC power injection on both DC-side and AC-side transient stability. During the simulation, a comparison is made on the DC fault analysis for when there is no power injection and when there is a DC power injection above and below the injection limit.

From the control setting parameters of the VSC HVDC transmission system in Simulink with a DC-link of 950 km, the following parameters were used to determine the injection limit:

$$U_{dcmax} = 1.05\,pu; \quad U_{dcref} = 0.95; U_{dc2} = 1.05\,pu; \quad I_{dc2} = 1.1\,pu; \quad r = 0.0139\,\Omega\,km, P_{ref} = 0.63.$$

Substituting the control and DC-link parameters in Eq. (1), the DC power injection limit can be calculated as 0.54 p.u. (162 MW).

During the simulation, a single-line-to-earth fault was applied on the positive line of the DC-link at 1.8 s, and the DC breaker opens at 1.9 s and closes at 2 s after the fault has been cleared in 1.92 s.

5.1. DC-side transient stability

Figures 11 and 12 show the DC-side transient response of the power and voltage, respectively. Comparing Figures 11a and 11b, it could be observed that the postfault power oscillation damped faster during power injection.

However, in Figure 11c, during power injection above the limit, P_{DC1} is seen to be reduced to 177 MW, showing that there is a reverse power flow to station 1, hence violating power stability.

Comparing Figures 12a and 12b, it can be seen that the oscillation of the voltage damped faster during the scenario of power injection below the limit, hence improving voltage stability in the postfault period. During power injection above the limit, it can be seen from Figure 12c that although the oscillation is damped faster, U_{DC1} and U_{DC2} are 387 kV and 371 kV respectively—more than the upper voltage regulation limit in p.u. specified in the control, and hence violating the voltage stability of the system.

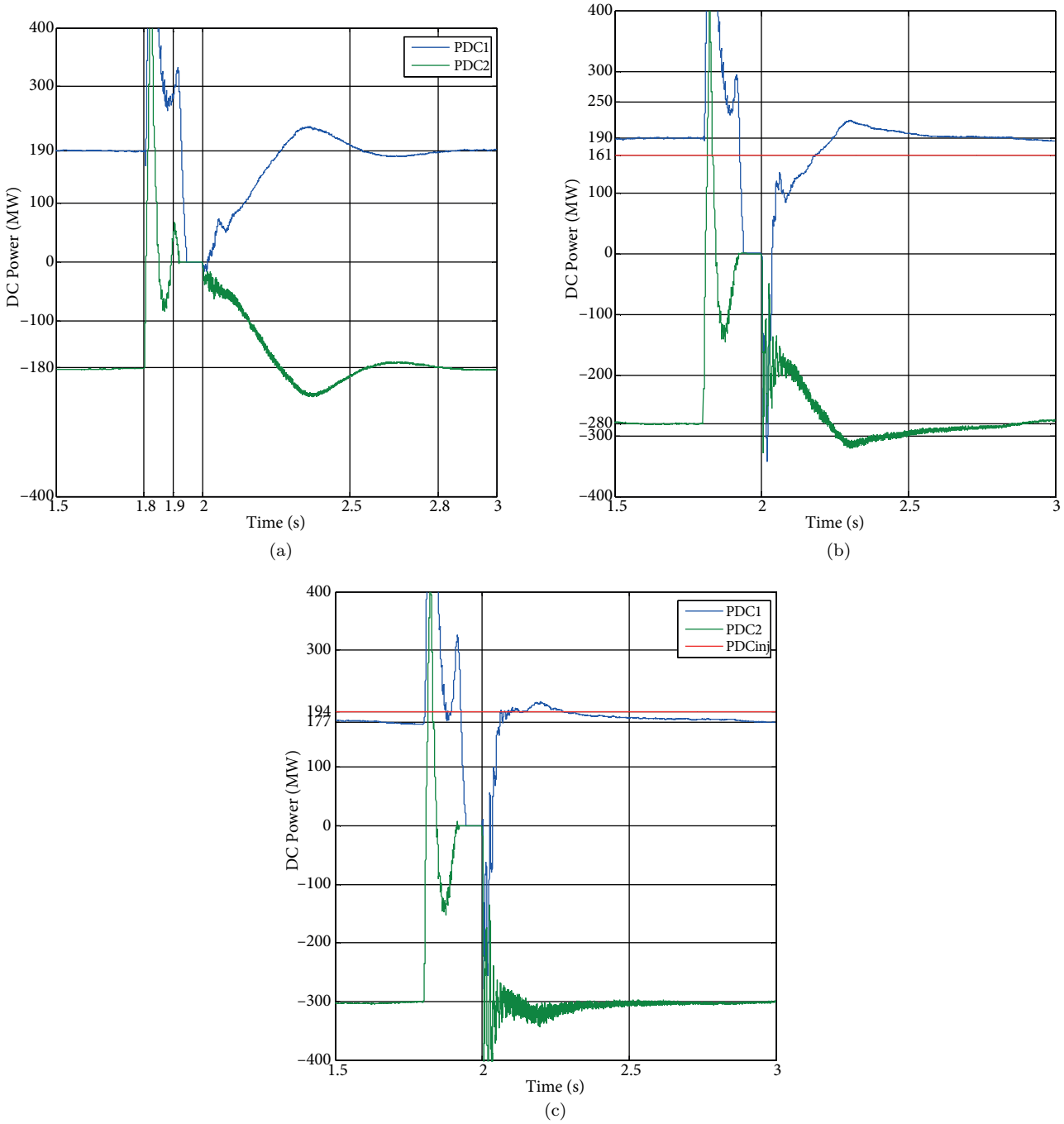

Figure 11. DC power response: a) no injection, b) injection (161 MW) below the limit, c) injection (194 MW) above the limit.

5.2. AC-side transient stability response

From Figure 13, it is observed that the load angle oscillates during the fault condition period and during the period that the breaker opens.

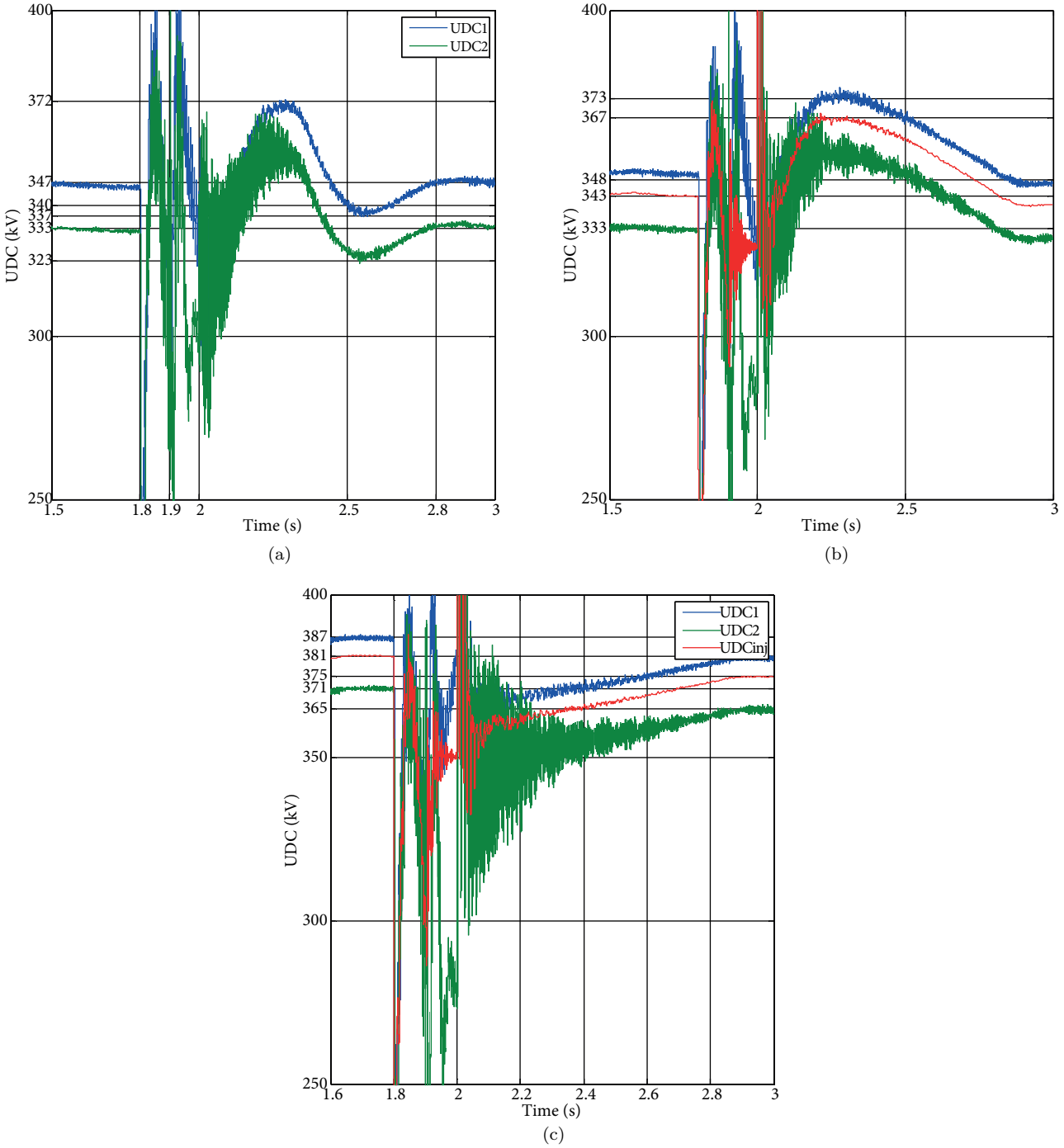

Figure 12. DC bus voltage response: a) no injection, b) injection (161 MW) below the limit, c) injection (194 MW) above the limit.

However, when the breaker closes at 2 s, the load angle oscillates and is damped faster during the injection scenario, hence improving the transient stability.

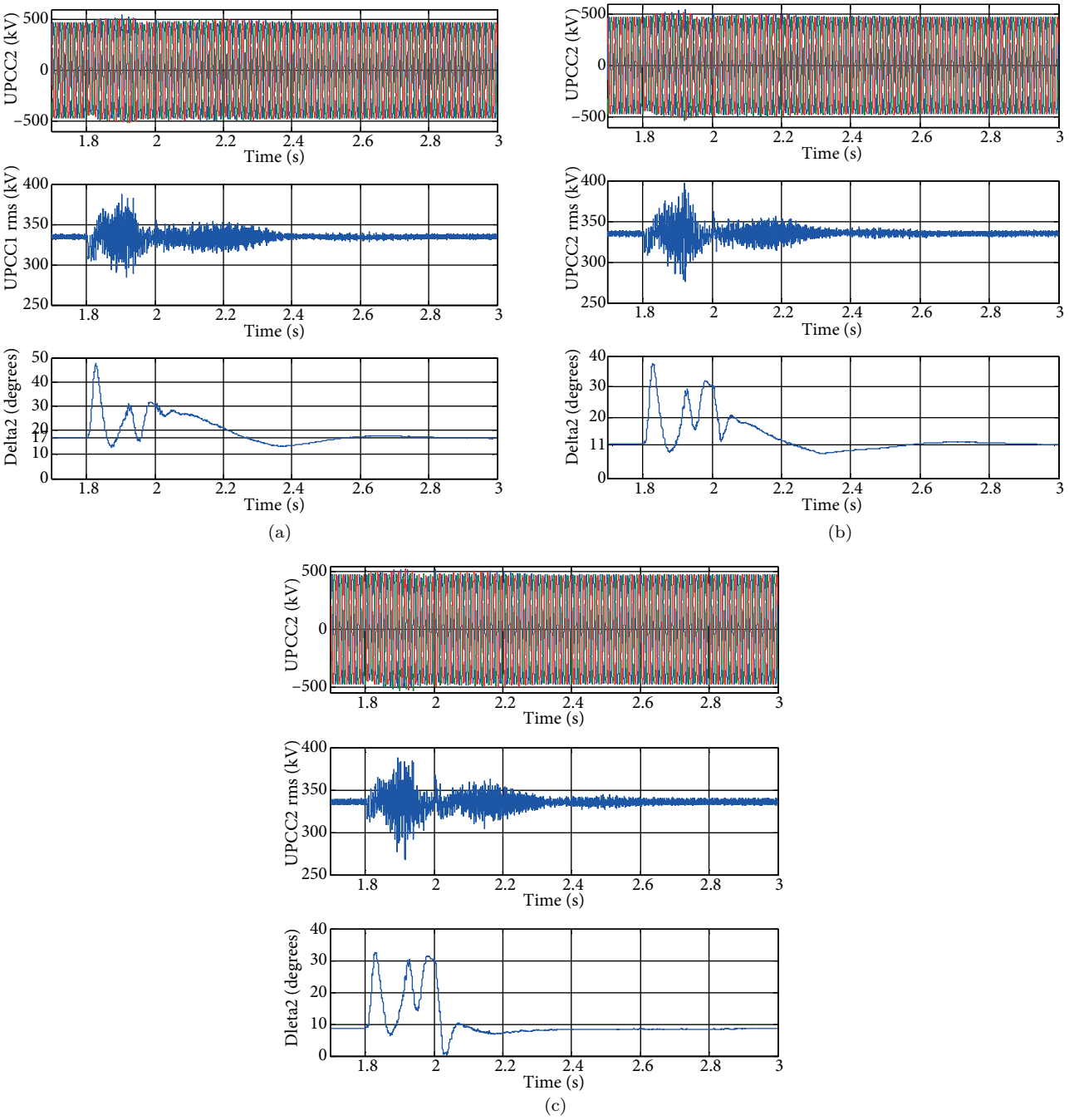

Figure 13. Station 2 UPCC and load angle: : a) no injection, b) injection below the limit, c) injection above the limit.

6. Conclusion

This paper presented the use of a DC-link of an embedded VSC HVDC transmission corridor to enhance the transient stability of an AC network by DC power injection on the DC-link. VSCs are vulnerable to DC cable short-circuits and ground faults due to the high discharge current from the DC-link capacitance. A DC line-to-earth fault results in a high DC fault current and blocks the VSC IGBTs, and hence the voltage source acts like an uncontrolled rectifier, which results in a rise in the AC fault current. In the analysis, a VSC HVDC

transmission having DC power injection on the DC-transmission corridor was modeled in the time domain. The zero-input zero-state (ZIZS) response was used to find the solution of the state-space representation. The system was also modeled in the MATLAB/Simulink environment. The results show that the power injection created an additional damping of the postfault oscillations of the AC-side power angle and the DC-side voltage and power oscillations, hence enhancing transient stability.

References

[1] Jiuping P, Reynaldo N, Tang L, Holmberg P. VSC-HVDC control and application in meshed AC network. In: IEEE 2008 Power and Energy Society General Meeting; 20–24 July 2008; Pittsburgh, Pennsylvania, USA. New York, NY, USA: IEEE. pp. 1–6.

[2] Alok K, Amar K. HVDC LIGHT and FACTS technology: a modern approach to power system interconnections. Int J Eng Res Appl 2012; 2: 1331–1336.

[3] Hamzei-Nejad A, Ong C. Coordinating the DC power injections of a multiterminal HVDC system for dynamic control of line flows. IEEE T Power Syst 1986; 1: 142–152.

[4] Du C, Bollen M, Agneholm E, Sannino A. A new control strategy of a VSC-HVDC system for high quality supply of industrial plant. IEEE T Power Deliver 2007; 22: 2386–2394.

[5] Bianchi F, Junyent-Ferre A, Gomis B. Droop control design for multi-terminal VSC-HVDC grids based on LMI optimization. IEEE T Power Deliver 2011; 26: 2476–2485.

[6] Gang S, Guoxiang W, Xu C, Zhe C. Coordinated control of multi-terminal VSC-HVDC transmission for large offshore windfarm. In: IEEE 2012 Power Electronics and Motion Control Conference; 2–5 June 2012; Harbin, Heilongjiang, China. New York, NY, USA: IEEE. pp. 1278–1282.

[7] Ruihua S, Chao Z. VSC based HVDC and its control strategy. In: IEEE 2005 Power and Energy Society Transmission and Distribution Conference & Exhibition; 18–20 December 2005; Dalian, Liaoning, China. New York, NY, USA: IEEE. pp. 1–6.

[8] Callavik M, Bahrman M, Sandeberg P. Technology developments and plans to solve operational challenges facilitating the HVDC Offshore Grid. In: IEEE 2012 Power and Energy Society General Meeting; 22–26 July 2012; San Diego, CA, USA. New York, NY, USA: IEEE. pp 1–6.

[9] Masters C. Voltage rise: the big issue when connecting embedded generation to long 11 kV overhead lines. Power Eng J 2002; 16: 5–12.

[10] Van Zyl S, Gaunt C. Generalised method for evaluating voltage rise in DG-equipped networks. In: CIGRE 2005 Distribution System and Dispersed Generation; 2005; Cape Town, South Africa.

[11] Nnachi AF, Munda JL, Nicolae DV, Mpanda Mabwe A. Power sensitivity and algebraic technique for evaluation of penetration level of photovoltaic on dc link of VSC HVDC transmission. In: IPEC 2012 10th International Power and Energy Conference; 12–14 December 2012; Ho Chi Minh City, Vietnam. New York, NY, USA: IEEE. pp. 121–126.

[12] Padiyar RK. FACTS: Controllers in Power Transmission and Distribution. 1st ed. Tunbridge Wells, UK: Anshan Publishers, 2009.

[13] Jiuping P, Nuqui, R, Srivastava, K, Jonsson, T, Holmberg, P, Hafner, YJ. AC grid with embedded VSC-HVDC for secure and efficient power delivery. In: IEEE 2008 Energy 2030 Conference; 17–18 November 2008; Atlanta, GA, USA. New York, NY, USA: IEEE. pp. 1–6.

[14] Chetty L, Ijumba N, Britten A. Parallel-cascaded tapping station. In: IEEE 2004 International Conference on Power System Technology; 21–24 November 2004. New York, NY, USA: IEEE. pp. 1874–1879.

[15] Rahman H, Khan B. Possibility of power tapping from composite ac-dc power transmission lines. IEEE T Power Deliver 2008; 23: 1464–1471.

[16] Nnachi AF, Munda JL, Nicolae DV, Mpanda Mabwe A. VSC HVDC transmission corridor: an option for PV power injection and AC network stability support. In: IEEE 2013 International Conference on Industrial Technology; 25–27 February 2013; Cape Town, South Africa. New York, NY, USA: IEEE. pp. 503–508.

[17] Yang J, Fletcher J, O'Reilly J. Multiterminal dc wind farm collection grid internal fault analysis and protection design. IEEE T Power Deliver 2010; 25: 2308–2318.

[18] Tang L, Ooi B. Protection of VSC-multi-terminal HVDC against DC Faults. In: IEEE 2002 Power Electronics Specialists Conference; 23–27 June 2002. New York, NY, USA: IEEE. pp. 719–724.

[19] Baran M, Mahajan N. Overcurrent protection on voltage-source-converter-based multiterminal DC distribution system. IEEE T Power Deliver 2007; 22: 406–412.

[20] Zhang L, Harnefors L, Rey P. Power system reliability and transfer capability improvement by VSC-HVDC (HVDC Light). In: CIGRE 2007 Conference on Security and Reliability of Electric Power Systems; 18–20 June 2007. Paris, France: CIGRE. pp. 1–7.

[21] Mousavi JM, Butler-Purry LK. A novel condition assessment system for underground distribution applications. IEEE T Power Syst 2009; 24: 115–1125.

[22] Rafferty J, Xu L, Morrow JD. DC fault analysis of VSC based multi-terminal HVDC systems. In: 10th IET 2012 International Conference on AC and DC Power Transmission; 4–5 December 2012; Birmingham, UK. London, UK: IET. pp. 1–6.

[23] Yang J, Fletcher JE, O'Reilly J. Multi-terminal DC wind farm collection grid internal fault analysis and protection design. IEEE T Power Deliver 2010; 25: 2308–2318.